Materials Advances

Accepted Manuscript

This article can be cited before page numbers have been issued, to do this please use: A. Nallathambi, V. S. Tiwari, E. Shai, E. Chiesa, I. Genta and M. Reches, *Mater. Adv.*, 2026, DOI: 10.1039/D6MA00253F.

ROYAL SOCIETY OF CHEMISTRY

rsc.li/materials-advances

DOI: 10.1039/D6MA00253F

Peptide-Functionalized Biomedical Polymers that Support Cell Adhesion and Prevent Bacterial Attachment

Abinaya Nallathambi[1,2], Vinay Tiwari[1], Ela Shai[3], Enrica Chiesa[2], Ida Genta[2*], Meital Reches[1 *]*

1. Institute of Chemistry and The Center for Nanoscience and Nanotechnology, The Hebrew University of Jerusalem, 9190401, Jerusalem, Israel
2. Department of Drug Sciences, University of Pavia, 27100, Pavia, Italy.
3. Department of Hematology; Hadassah Hebrew University Medical Center, Jerusalem, 9112001, Israel.

E-mail: enrica.chiesa@unipv.it; ida.genta@unipv.it; meital.reches@mail.huji.ac.il

Keywords: Peptide-functionalized polymers, Antifouling, Electrospun scaffolds, DOPA, RGD peptide, implants, peptide self-assembly

Abstract

The demand for multifunctional biomaterials drives the development of medical polymers from passive support to active scaffolds in infection control and tissue regeneration. To address antimicrobial resistance and implant rejection, we generated peptide-functionalized scaffolds using electrospun polyurethane (PU) and poly(L-lactide-co-caprolactone) (PLC). We synthesized two peptides containing 3,4-dihydroxyphenylalanine (DOPA) for stable surface immobilization: one providing antifouling activity, and the other combining antifouling activity with the adhesive Arg-Gly-Asp (RGD) motif to promote cell adhesion. X-ray photoelectron spectroscopy and FTIR spectroscopy confirmed the peptide attachment to the polymers. Both peptides reduced bacterial adhesion by ~90%. The RGD-functionalized peptide enhanced cell adhesion by over 400% on PU, while PLC scaffolds maintained similar cell compatibility with the peptide-functionalized scaffolds. Hemocompatibility tests showed minimal hemolysis and thrombus formation, supporting use in blood-contacting applications. We also report the application of enzymatic cleavage coupled with Liquid Chromatography-Mass Spectrometry (LC-MS) for quantifying peptide surface density on biomedical scaffolds. These results demonstrate the promise of peptide-functionalized scaffolds in biomedical implant applications.

View Article Online
DOI: 10.1039/D6MA00253F

Introduction

Biomedical implants such as heart valves substitutes (e.g., bileaflet valve, porcine or bovine valves), joint prostheses, and vascular catheters have significantly advanced patient care by restoring function and extending life expectancy. However, the clinical success of these devices is often compromised by serious complications, including chronic inflammation, foreign body responses, thrombosis, and, most critically, infection arising from microbial colonization at the implant site. These complications not only hinder tissue integration and functional recovery but also pose risks of implant failure and systemic illness, often requiring revision surgeries or device removal. Among these, infections pose one of the most serious threats not only due to their prevalence but because conventional treatments often fail [1-5]. Once bacteria colonize implant surfaces, they form biofilms, structured communities encased in a protective matrix that shields them from antibiotics and immune responses. This biofilm-mediated resistance renders standard antimicrobial therapies ineffective, frequently necessitating surgical removal or replacement of the implant thus, life-saving medical devices can paradoxically become conduits for deadly infections.[6] Frequent culprits, such as *Staphylococcus aureus* (*S.aureus*) and *Staphylococcus epidermidis* (*S.epidermidis*), are consistently identified in literature as primary pathogens associated with implant-related infections, including endocarditis in prosthetic heart valves.[7-10] Their ability to rapidly colonize biomaterial surfaces and form antibiotic-resistant biofilms presents a major clinical challenge.

To address these limitations, we present a surface biofunctionalization strategy using rationally designed peptides to confer antifouling and regenerative properties to implantable polymeric scaffolds. These peptides are engineered to simultaneously suppress non-specific protein adsorption and bacterial adhesion, while promoting mammalian cell attachment. A key design element is the incorporation of a catechol-bearing DOPA residue, inspired by mussel adhesive proteins, which enables strong, water-stable anchoring of peptides to polymer surfaces. [11-13] The antifouling behavior is attributed to the fluorinated residues that lower the surface energy and impede microbial attachment, while the Phe(4F)-Phe(4F) motif facilitates the self-assembly of the peptide on surfaces [14]. One peptide variant included RGD, a well established motif that promotes integrin-mediated cell adhesion.[15-18] Our previous studies have demonstrated the effect of each individual element including DOPA at various locations in the peptide sequence as well as scrambled RGD [18-21]

In this study, we present the development of next-generation biomaterials designed to resist biofouling while promoting tissue integration. The engineering of advanced materials

View Article Online
DOI: 10.1039/D6MA00253F

increasingly depends on the ability to modulate surface interactions at the molecular level. We focused on medical-grade polymers such as polyurethanes (PU)—widely used in catheters, wound dressings, heart valves, and skin sensors [22, 23] and poly(L-lactide-co-ε-caprolactone) (PLC), which is gaining prominence in tissue engineering for implantable applications due to its favorable mechanical properties, biocompatibility, and processability. [24, 25]

We employed electrospinning as our fabrication method due to its superior adaptability for biomedical applications such as vascular grafts, wound dressings, and implant coatings. Compared to techniques like solvent casting, electrospinning enables the production of nanofibrous architectures that closely mimic the structural features of natural tissue.[26] Electrospun mats provide a high surface-area-to-volume ratio and tunable fiber alignment and porosity, making them particularly well-suited for biomedical applications where surface interactions are critical.[27, 28] Despite their advantageous properties, these polymers are inherently bioinert, lacking the functional cues necessary to promote selective cell adhesion or effectively resist microbial colonization. To overcome these limitations, bioactive peptide coating provides a versatile and precise means to tailor surface functionality, enhancing both cellular engagement and antimicrobial performance. This approach is particularly critical given the escalating global threat of antimicrobial resistance (AMR), as emphasized by the World Health Organization, underscoring the urgent need for innovative strategies to prevent device-associated infections caused by priority AMR pathogens.[1, 29, 30]

2. Results and Discussion

2.1. Peptide synthesis and coating characterization

We synthesized the peptides DOPA-Phe(4F)-Phe(4F)-OMe (termed TP) [16] and NH_2-DOPA-Phe(4F)-Phe(4F)-Arg-Gly-Asp-NH_2 (termed HP), which exhibits antifouling activity with enhanced cell adhesion via its RGD motifs [18, 21]. In this study, we applied these peptides to two structurally and functionally distinct polymer substrates: PU, a non-degradable material widely used in catheters and blood-contacting devices, and PLC, a biodegradable polymer increasingly utilized in tissue engineering. By selecting both degradable and non-degradable scaffolds, we sought to evaluate the versatility and efficacy of peptide-based surface functionalization across a spectrum of biomedical applications requiring both antifouling protection and cellular bioactivity. Electrospinning of PU (5% w/v in HFIP) and PLC (20% w/v in DCM) solutions performed under controlled conditions (27 °C, 35% relative humidity) to produce

View Article Online
DOI: 10.1039/D6MA00253F

uniform, reproducible nanofibrous scaffolds. Electrospun PLC and PU scaffolds, with an average fiber diameter of 2.0 ± 1.0 μm and 0.8 ± 0.4 μm, respectively (Fig S1), were chosen based on optimized morphologies established in our previous work. These fibers have high surface area suitable for peptide adsorption. Scaffolds were cut into pieces of 1 cm² and surface-functionalized by immersing them for 48 hr. at room temperature in the peptide solution: TP in ethanol and HP in Tris buffer (pH 7.4, 154 mM) each at a concentration of 1 mg/mL. After incubation, scaffolds were rinsed with ethanol to remove unbound peptides and dried under nitrogen. HP is insoluble in ethanol; Tris buffer was used to provide suitable pH and ionic strength for DOPA-mediated immobilization. We tested initial washes with water but did not detect any difference; therefore, a standardized ethanol wash protocol was adopted for consistency.

SEM analysis confirmed that peptide functionalization did not significantly alter the morphology of the scaffolds. Post-treatment measurements showed consistent fiber diameters of 1.7 ± 0.9 μm for PLC and 0.7 ± 0.2 μm for PU, demonstrating structural preservation, as shown in Fig S2. The water contact angle measured immediately was 120°, 86° and 42° for PU, PU coated with the tripeptide and PU coated with the hexapeptide respectively. Due to the low adsorption levels and small molecular size of the peptides, their direct visualization on the surface of the fibers is challenging. Therefore, X-ray photoelectron spectroscopy (XPS) was employed to confirm peptide immobilization, which detected distinct fluorine peaks. Distinct fluorine peaks (685–690 eV) were detected on both PU and PLC scaffolds **(Fig 1a)**, confirming the successful surface functionalization. We determined the optimal immersion time by testing PU scaffolds in peptide solutions for 4, 12, 24, and 48 hours, followed by ethanol washing to remove unattached peptides. XPS analysis showed a time-dependent increase in the fluorine signal intensity over the tested period, with 48 hours **(Fig. 1b)** providing a practical balance between performance and process feasibility.

To assess long-term coating stability, peptide-functionalized PU and PLC scaffolds were immersed in PBS for eight weeks. XPS analysis showed that fluorine signals remained detectable, indicating sustained peptide retention, with material- and peptide-dependent differences reflected in the F/O ratios (Table S1).

View Article Online
DOI: 10.1039/D6MA00253F

To analyze the nature of peptide–scaffold interactions, Fourier Transform Infrared (FTIR) spectroscopy was employed (**Fig 1c**). For the hexapeptide-functionalized PLC (HP_PLC), a broad absorption band appeared at 3189 cm^{-1}, corresponding to N–H and/or O–H stretching vibrations. This suggests the formation of hydrogen bonds between the peptide moieties and the polymer surface. Additionally, notable shifts in the amide bands were observed: the amide II band shifted from 1511 cm^{-1} to 1553 cm^{-1}, and the amide I band shifted from 1601 cm^{-1} to 1630 cm^{-1}. These spectral changes are consistent with peptide adsorption via non-covalent interactions, such as hydrogen bonding and π–π stacking.[18, 21] In contrast, tripeptide-functionalized PLC (TP_PLC) showed minimal or overlapping spectral changes, possibly due to lower surface density or weak infrared absorption.

For the PU scaffolds, HP_PU, a distinct doublet emerged around 1076 cm^{-1}, replacing the single peak with a shoulder observed in the control, suggesting conformational heterogeneity introduced by peptide binding, particularly affecting C–O stretching vibrations. Similarly, for TP_PU, two resolved N–H stretching peaks at 3320 cm^{-1} and 3190 cm^{-1} replaced the broad band seen in the control, indicating enhanced hydrogen bonding and altered local environments. The amide I region broadened significantly in TP_PU, shifting from a sharp peak at 1595 cm^{-1} (with a shoulder at 1610 cm^{-1}) to a broad envelope extending up to 1652 cm^{-1}, consistent with ordered secondary structure formation such as β-sheets [31], Furthermore, C–O stretching peaks appeared at 1037 cm^{-1} and 1106 cm^{-1} in the functionalized samples, replacing the single control peak at 1075 cm^{-1}. These findings support the presence of DOPA-based peptide assemblies, where catechol-mediated adhesion induces broad N–H/O–H peaks and amide shifts indicative of non-covalent bonding [32]. For reference, the FTIR spectra of the free peptides—DOPA–Phe(4F)–Phe(4F)–OMe (TP) and NH_2–DOPA–Phe(4F)–Phe(4F)–RGD–$CONH_2$—are shown in Fig.S3, enabling direct comparison with the peptide-functionalized polymer samples.

Although FTIR analysis provided indication of peptide presence, the signals were subtle and difficult to resolve due to overlapping with native polymer peaks. Therefore, FTIR alone was insufficient for conclusive characterization and was complemented with the

View Article Online
DOI: 10.1039/D6MA00253F

XPS analysis. In addition, we quantified the number of surface-attached peptides using the following procedure.

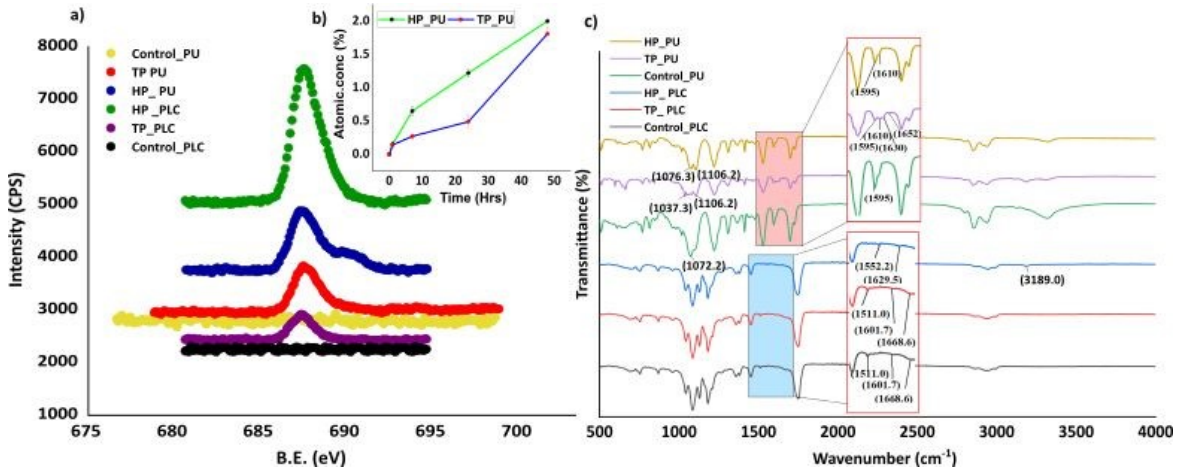

Fig 1. Surface analysis of peptide-functionalized electrospun scaffolds. (a) XPS spectra show characteristic fluorine peaks at binding energy 685–690 eV, confirming successful immobilization of fluorinated peptides on PU and PLC surfaces. (b) Time-dependent XPS quantification reveals increasing surface fluorine intensity over 48 hr, indicating progressive peptide adsorption. 3 (c) ATR-FTIR spectra reveal peptide–scaffold interactions with no disruption to the polymer backbone. New N–H/O–H and C–O stretching peaks, along with amide I/II shifts, suggest hydrogen bonding and non-covalent peptide attachment. Standard deviation represents the variability across three independently acquired measurement spots, with values reported as mean ± SD.

2.2. Quantification of surface-attached peptides

Accurate quantification of immobilized peptide surface density remains a significant challenge in biomaterial characterization, with no well-established analytical methods currently available. While the Enzymatic digestion coupled with LC-MS is a powerful tool in proteomics and bioanalysis [33] its application has mostly been limited to soluble proteins or removing templates from polymers rather than directly quantifying surface-bound peptides.[34] We employed an enzymatic cleavage method using Proteinase K, uniquely optimized to release peptides immobilized on scaffold surfaces, followed by LC-MS analysis to determine their absolute surface density. This approach enables sensitive and direct quantification in units such as pmol cm^{-2}, facilitating reliable comparisons of scaffold functionalization levels. Unlike surface digestion methods aimed at probing protein orientation on biosensors,[35] our method focuses specifically on extracting functional peptide payloads for quantitative evaluation. To our knowledge, this is the first study to apply enzymatic cleavage coupled with LC-MS for accurate, absolute quantification of peptides on biomaterial scaffolds (Table 1).

View Article Online
DOI: 10.1039/D6MA00253F

Proteinase K-based is a broad-spectrum serine protease capable of hydrolyzing peptide bonds involving aliphatic, aromatic, and hydrophobic residues such as phenylalanine.[36] Enzymatic digestion was performed using Proteinase K (1 mg/mL) in a solution containing 5 mM ascorbic acid and 5 mM $CaCl_2$. Ascorbic acid served to protect DOPA-containing peptides from oxidative degradation, while $CaCl_2$ acted as a cofactor to enhance the enzymatic activity of Proteinase K.[37] Post-digestion, cleaved 4F-phenylalanine (4F-Phe) residues were extracted using the extraction buffer (MeOH:MeCN:H_2O, 5:3:2) and quantified by LC-MS, allowing accurate estimation of surface-bound peptide content. This method is applicable to any cleaved amino acid; however, 4F-Phe was selected due to its fluorinated structure, enabling both selective detection and correlation with XPS fluorine trends, thereby reinforcing the reliability and robustness of the quantification method. The method achieved ~84% cleavage efficiency, with residual fluorine signals detected by XPS (Table S2), indicating a minor peptide fraction that remained strongly associated with the surface, potentially requiring extended digestion or further optimization.

From an alternative perspective, even after 4 hours of exposure to a high concentration of proteinase K (1 mg/mL), approximately 20% of the peptide remained undigested. The residual peptide signal after digestion may be attributed to limited enzyme accessibility caused by strong interfacial binding, steric hindrance, and possible oxidation-driven stabilization of DOPA-containing species [38]

Proteinase K is not a physiological enzyme, [39] and the chosen concentrations far exceed those typically found in the body; it likely overestimates actual *in vivo* degradation. Since the electrospun graft intended for application in cardiac valve replacement, it will be exposed primarily to endogenous proteases such as matrix metalloproteinases (MMP-2, MMP-9), cathepsins, and elastase enzymes that participate in tissue remodeling and inflammatory responses. These enzymes are typically present at much lower concentrations, in the nanogram-per-milliliter range. [40-42] The persistence of the peptide coating under harsh proteolytic conditions thus underscores its structural stability and supports its potential for long-term durability in physiological environments.

Table 1. Quantification of surface-immobilized peptides on PU and PLC scaffolds. Peptide amounts were determined via enzymatic cleavage followed by LC-MS analysis using 4-

View Article Online
DOI: 10.1039/D6MA00253F

fluorophenylalanine (4F-Phe) as a peptide marker. The data normalized to sample optical density (OD), with averages calculated from three replicates (n = 3)

Sample Name	4F-Phe [μmoles/cm²]	RSD [%]
TP_PLC	2.25	0.71
HP_ PLC	0.579	2.86
TP_PU	0.010	7.60
HP_PU	0.250	2.94

a) (RSD-Relative standard deviations)

The table presents the absolute concentrations of 4F-Phe released from different scaffold types. The data show higher peptide quantities on PLC scaffolds compared to PU, underscoring the influence of polymer surface chemistry. PU used here is the medical-grade thermoplastic polyurethane composed of segmented hard methylene diphenyl diisocyanate (MDI) and 1,4-butanediol (BDO) chain extenders and the soft segments are formed from poly (tetramethylene ether) glycol (PTMEG),[43] resulting in a predominantly hydrophobic and relatively inert surface with limited reactive groups for peptide anchoring. The HP exhibited significantly higher retention (0.25 μmoles/cm^2) than the TP (0.01 μmoles/cm^2), which is attributed to the increased number of polar and charged residues in the RGD motif, facilitating enhanced hydrogen bonding and electrostatic interactions with the urethane hard segments. Both peptides contain fluorinated phenylalanine residues that contribute hydrophobic interactions with the soft PTMEG segments, and the DOPA moiety promotes adhesion via catechol-mediated hydrogen bonding.[44] The longer hexapeptide likely achieves greater conformational flexibility and surface coverage, thereby maximizing scaffold interaction and retention. In contrast, the shorter tripeptide has limited interaction sites and conformational adaptability, leading to reduced affinity. This is in agreement with our previously reported paper that show that other factors can affect the surface coverage such as high electronegativity and absence of the self-assembled motif .[18]

PLC is a biodegradable elastomeric copolymer composed of hydrophobic ε-caprolactone and more hydrophilic L-lactide units, conferring a relatively more hydrophilic and ester-rich surface chemistry that facilitates effective peptide anchoring.[45] Additionally, TP exhibited greater surface retention than HP, likely due to their smaller molecular size and enhanced surface accessibility, while steric hindrance could limit hexapeptide immobilization.[46]Thus, the opposite trends observed in PU and PLC are consistent with their differing hydrophobicity, functional group availability, and steric constraints rather than experimental variability. Although FTIR analysis of TP_PLC did not reveal notable

View Article Online
DOI: 10.1039/D6MA00253F

spectral shifts, LC-MS confirmed high peptide loading. This apparent discrepancy can be attributed to the limited surface sensitivity of FTIR,[47] where dominant polymer backbone bands may obscure the weak signals arising from a thin peptide layer, particularly when the peptide is non-covalently bound and present at low surface density. By contrast, LC-MS relies on peptide extraction into solution followed by highly sensitive mass-based detection,[48] allowing selective identification and quantification with minimal interference from the polymer matrix.

2.3. Antifouling studies

The antifouling performance of TP and HP coatings on two polymeric substrates, namely HP_PU, TP_PU, and HP_PLC, TP_PLC, was quantitatively analyzed using three clinically relevant bacterial strains: *Escherichia coli (E.coli)*, *Staphylococcus epidermidis (S. epidermidis)*, and *Staphylococcus aureus (S.aureus)*. TP_PU surfaces exhibited approximately 90% reduction in bacterial attachment across all strains. HP_PU showed reductions of 63%, 88%, and 94% for *E. coli*, *S. epidermidis*, and *S. aureus*, respectively. On PLC substrates, TP-modified surfaces achieved 93%, 90%, and 87% reductions, while HP_PLC surfaces achieved 92%, 84%, and 92% bacterial inhibition, respectively. These findings, summarized in **Fig 2**, underscore the strong antifouling efficacy of both peptides. Although numerical differences in bacterial inhibition noted between TP and HP coatings, no statistically significant difference found between them on the same peptide-polymer type, suggesting comparable performance. In contrast, both peptide-coated surfaces showed substantial reductions in bacterial adhesion compared to their unmodified counterparts.

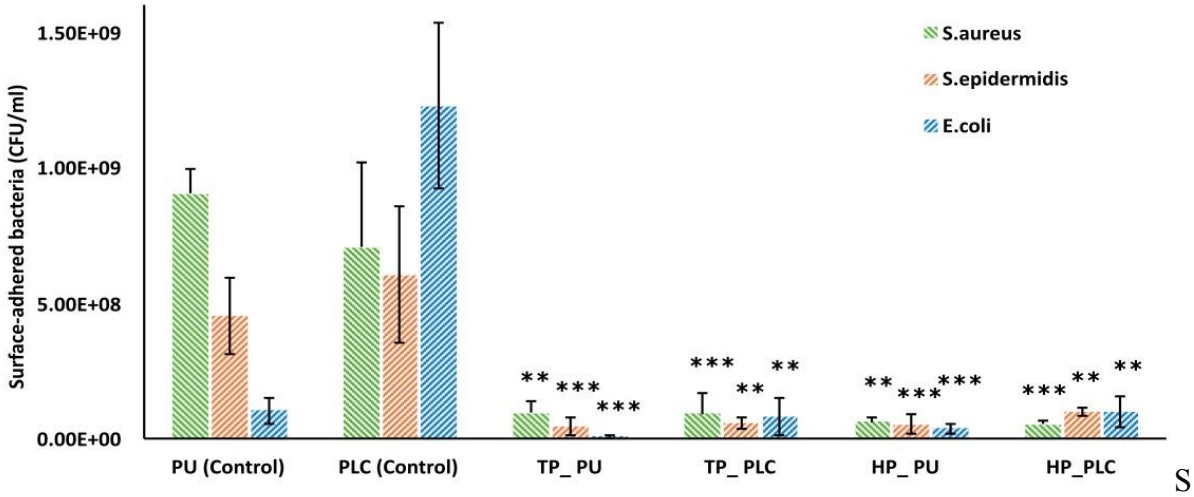

S

Fig 2. Antifouling studies showing reduced microbial attachment on electrospun PU and PLC polymer surfaces. Functionalization with tripeptide (TP) and hexapeptide (HP)

View Article Online
DOI: 10.1039/D6MA00253F

significantly reduced bacterial attachment compared to unmodified surfaces. Bacterial attachment assessed for (a) *Staphylococcus aureus* (Gram-positive, coagulase-positive), (b) *Staphylococcus epidermidis* (Gram-positive, coagulase-negative), and (c) *Escherichia coli* (Gram-negative). Data presented as mean ± SD ($n = 3$ technical replicates per condition; $N = 3$ independent biological repeats). Statistical significance is determined using one-way ANOVA with Tukey–Kramer post hoc test (*$p < 0.05$, **$p < 0.01$, ***$p < 0.001$).

Corroborative SEM analysis provided visual confirmation of the antifouling effect. Representative SEM micrographs **(Fig 3)** illustrate substantial reductions in bacterial colonization on peptide-functionalized surfaces relative to uncoated controls. Images captured before ultrasonic washing to preserve the native attachment patterns. *S. epidermidis* and *E. coli* visualized. Observations for *S. aureus* closely mirror *S. epidermidis in* the Supplementary (Fig S4). The marked decrease in surface-associated bacteria is attributed to the fluorinated phenylalanine residues in the peptide sequence, which enhances hydrophobicity, in conjunction with the inherently hydrophobic nature of the PU and PLC substrates. Together, these features synergistically contribute to the observed antifouling behavior.

View Article Online
DOI: 10.1039/D6MA00253F

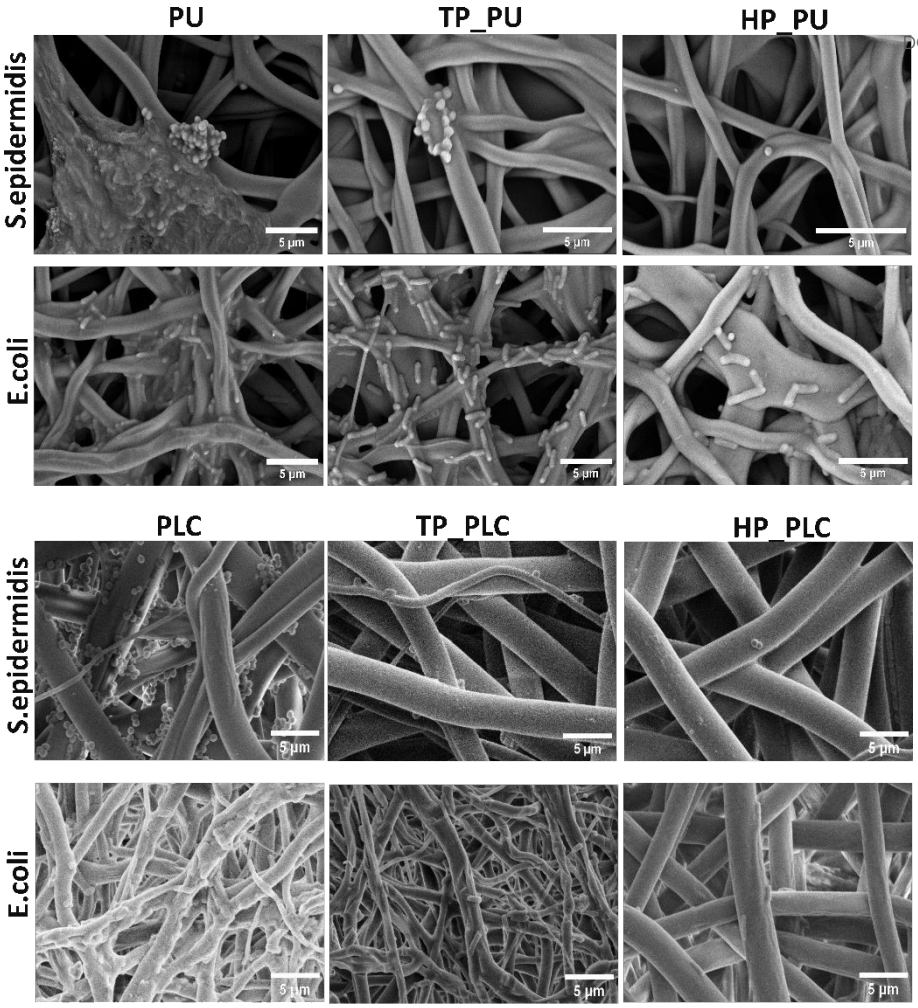

Fig 3. SEM micrographs showing bacterial attachment on peptide-functionalized and unmodified scaffolds. Representative SEM images show *the adhesion of S. epidermidis and E. coli* on PU and PLC scaffolds, both unmodified (control) and peptide-functionalized, before ultrasonication. Unmodified scaffolds exhibit extensive bacterial colonization and visible biofilm formation, particularly on PU. In contrast, peptide-coated surfaces show markedly reduced bacterial attachment, supporting the antifouling effect observed in quantitative assays. Each scaffold was tested in triplicate (N = 3), with SEM images collected at least 5 random regions per sample

Although there are decoupling factors between surface chemistry, substrate properties, and peptide loading, here, we wanted to establish a versatile application on different surfaces by exploiting the strong and universal adhesion capability of DOPA.

DOPA mediates robust attachment to a wide range of materials through catechol–surface interactions, including hydrogen bonding, metal coordination, and π–π stacking, enabling stable functionalization even under aqueous conditions [49, 50]. A maximum concentration of 1 mg/mL was therefore used to attain better peptide coverage on the surface, while recognizing that the absolute amount of attachment differs depending on the underlying substrate chemistry. Despite

View Article Online
DOI: 10.1039/D6MA00253F

these variations, the antifouling performance is preserved across the tested surfaces, indicating that DOPA-based functionalization can effectively support the desired application without compromising the primary goal of fouling resistance. The presence of fluorine-containing residues supports the notion that even minimal surface coverage of a few nanomolar per square centimeter is sufficient to impart significant antifouling properties. Furthermore, the inclusion of the RGD motif, known for promoting mammalian cell adhesion via integrin binding, did not enhance bacterial attachment, indicating a degree of selective bio-interactivity.[18]

2.4. Cell adhesion and proliferation studies

Cell–material interactions are critical determinants of implant integration, macrophage recruitment, inflammatory cascade activation, fibrous encapsulation, and eventual implant integration or rejection.[51] To evaluate the cytocompatibility of peptide-functionalized polymeric scaffolds, Chinese Hamster Ovary (CHO) cells were employed as a standard mammalian cell line per ISO 10993-5:2009 guidelines for biological evaluation of medical devices. [52] A seeding density of 25,000 cells per well selected to ensure adequate surface coverage and to simulate early-stage implant contact with mammalian cells. The cells were incubated for 72 hours, allowing sufficient time for adhesion and proliferation before analysis using the trypan blue exclusion assay. This assay was chosen for its rapidity, cost-effectiveness, and suitability for high-throughput applications in early biocompatibility screening.[53] We initially attempted standard viability assays, including fluorescence-based staining and MTT; however, these methods were not suitable for the electrospun scaffolds due to significant interference arising from the absorbent nature of the polymer matrix and the intrinsic fluorescence of the peptide. Consequently, Trypan Blue staining was employed as a more reliable alternative. High-resolution SEM was employed in parallel to visualize cell morphology and attachment. SEM images provided qualitative confirmation of cell viability, revealing distinct morphologies across different surfaces. Control surfaces exhibited non-spread cells indicative of poor attachment or viability. However, high cell density led to image crowding, limiting precise quantitative analysis**.** In contrast, peptide-coated surfaces—particularly those functionalized with hexapeptide—exhibited more spread out on the surface cells with extended filopodia, lamellipodia.

Quantitative and qualitative assessments in **Fig 4** demonstrated enhanced cell adhesion on HP_PU, which incorporate an RGD motif known to facilitate integrin-mediated binding and promote cellular anchorage to biomaterials.[54] The HP_PU surface

View Article Online
DOI: 10.1039/D6MA00253F

demonstrated a statistically significant increase in the live cells with a count of 400% compared to the control. This highlights its superior cell-supportive capability as the TP_PU surface showed an increase of 130% relative to the control. This improvement was not statistically significant, emphasizing the crucial role of the RGD motif in enhancing cell interactions. Nonetheless, the TP coating demonstrated comparable biocompatibility to the control, with no evidence of cytotoxicity or adverse cellular responses. Although a higher number of dead cells was observed on HP_PU, the absolute values were still very low (on the order of 10^3 cells) and were negligible relative to the substantially elevated live cell population. This indicates that the increased dead cell count is likely associated with higher cell density and confluence rather than any cytotoxic effect. Consistently, the TP coating demonstrated comparable biocompatibility to the control, with no evidence of cytotoxicity or adverse cellular responses.

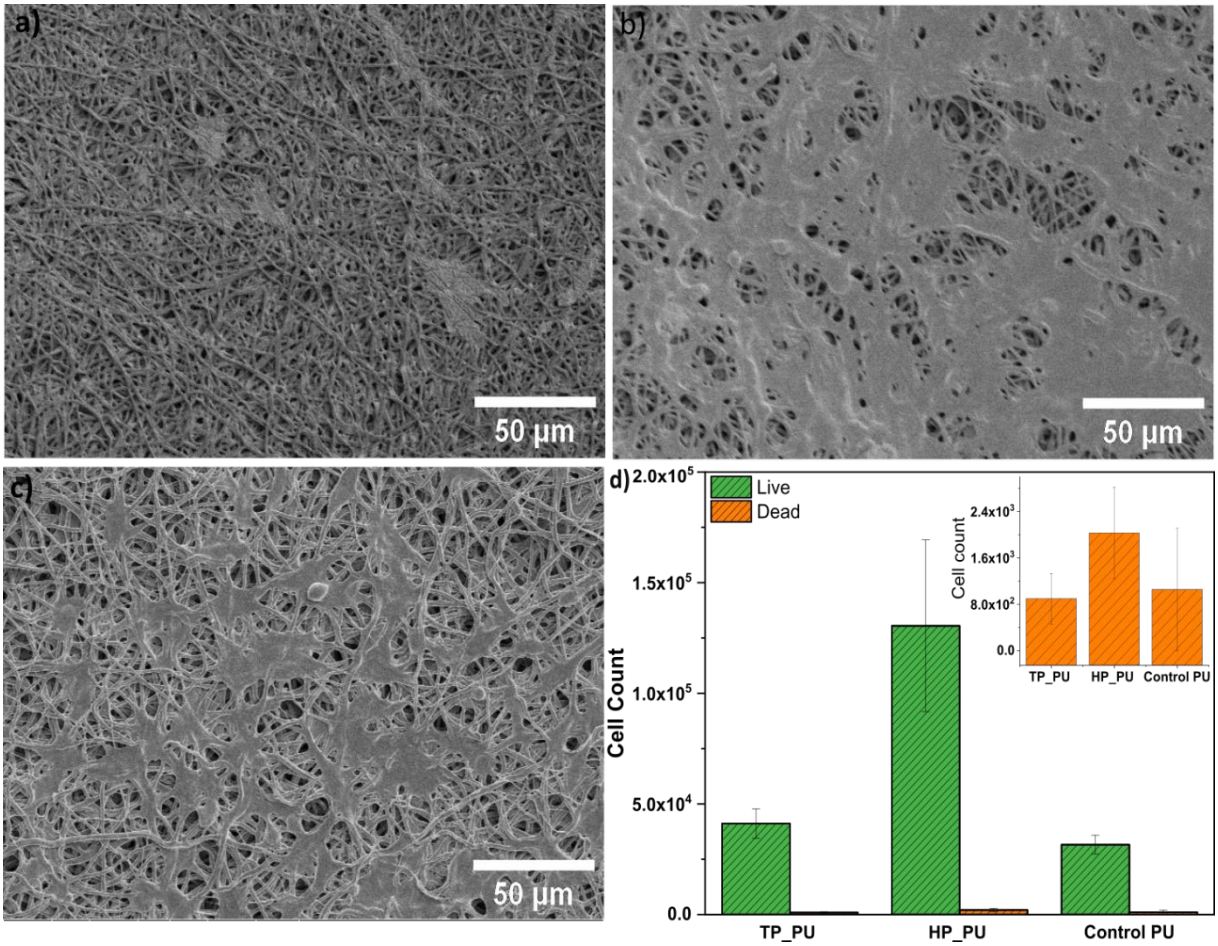

Fig 4. CHO cell adhesion and proliferation on electrospun PU scaffolds.
(a–c) SEM images of CHO cells cultured on PU scaffolds functionalized with (a) tripeptide (TP), (b) hexapeptide (HP), and (c) unmodified control. HP-functionalized scaffolds show enhanced cell adhesion, spreading, and morphological development, indicating superior bioactivity compared to TP and control surfaces. (d) Quantitative analysis of CHO cell adhesion using the trypan blue exclusion assay after trypsinization. Viable cells counted with a hemocytometer reveal significantly higher adhesion on HP-modified scaffolds (containing

View Article Online
DOI: 10.1039/D6MA00253F

RGD motifs). Statistical analysis: Student's t-test; ns: not significant ($p > 0.05$), *$p < 0.05$, **$p < 0.01$, ***$p < 0.001$. Data presented as mean ± SD (n = 3 technical replicates per condition; N = 3 independent biological repeats).

PLC surfaces functionalized with both peptides in **Fig 5** also showed comparable viability, with live cell coverage reaching 154% of the control for HP and 137% of the control for TP. However, unlike PU, PLC did not exhibit a marked difference between hexapeptide and control. This may be attributed to the fact that both the control and peptide-functionalized PLC surfaces already supported substantial and comparable cell growth. The uniformity in cellular response across all PLC samples suggests that the base material itself is highly biocompatible, and peptide functionalization did not significantly alter the cell adhesion or proliferation outcomes in this case. Although a higher number of dead cells observed, particularly on TP_PLC surfaces, this is attributable to increased cell confluence or density, resulting in competition for space and nutrients, rather than any cytotoxic effects of the coating. Notably, despite this visual observation, the number of dead cells was ultimately statistically lower.

The incorporation of the RGD integrin recognition motif into the hexapeptide sequence is intended to mimic extracellular matrix cues, which may enhance cellular attachment and support a favorable tissue response.[55] This bio-interactive design strategy could potentially contribute to reduced immune rejection and improved long-term implant integration. although further studies are needed to confirm these effects.

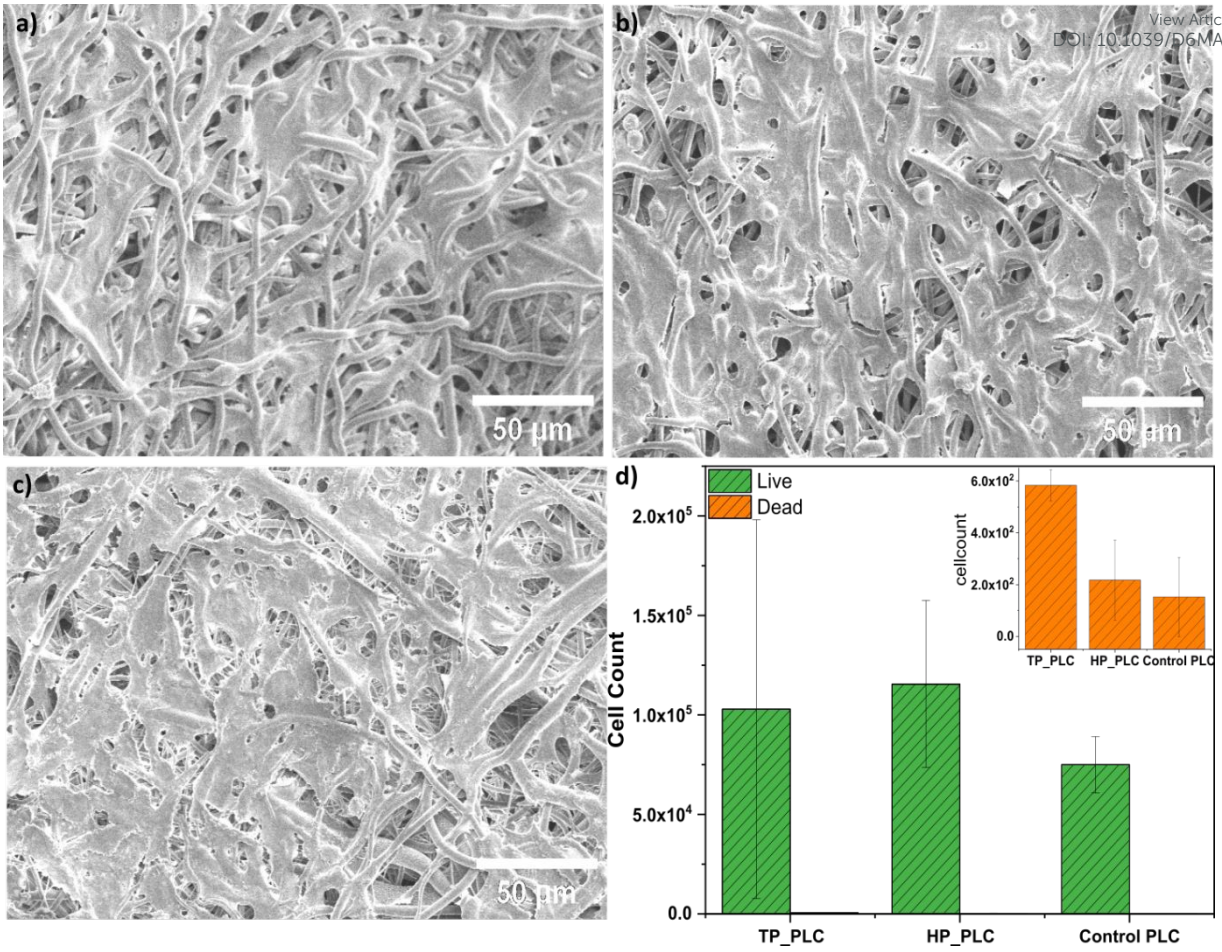

Fig 5. CHO cell adhesion and proliferation on electrospun PLC scaffolds.
(a–c) SEM images of CHO cells cultured on PLC scaffolds functionalized with (a) tripeptide (TP), (b) hexapeptide (HP), and (c) unmodified control. All conditions show comparable cell adhesion, spreading, and morphology, indicating preserved biocompatibility across treatments. (d) Quantitative analysis of CHO cell adhesion using the trypan blue exclusion assay after trypsinization. Viable cells counted with a hemocytometer reveal no statistically significant differences among the groups, indicating that peptide functionalization does not adversely affect PLC scaffold biocompatibility. Statistical analysis performed using Student's t-test; ns: not significant ($p > 0.05$), *$p < 0.05$, **$p < 0.01$, **$p < 0.001$. Data presented as mean ± SD ($n = 3$ technical replicates per condition; $N = 3$ independent biological repeats).

Although there are decoupling factors between surface chemistry, substrate properties, and peptide loading, here, we wanted to establish a versatile application on different surfaces by exploiting the strong and universal adhesion capability of DOPA.

DOPA mediates robust attachment to a wide range of materials through catechol–surface interactions, including hydrogen bonding, metal coordination, and π–π stacking, enabling stable functionalization even under aqueous conditions.[49, 50] A maximum concentration of 1 mg/mL was therefore used to attain better peptide coverage on the surface, while recognizing that the absolute amount of attachment differs depending on the underlying substrate chemistry. Despite these variations, the antifouling performance is preserved across the tested surfaces, indicating

View Article Online
DOI: 10.1039/D6MA00253F

that DOPA-based functionalization can effectively support the desired application without compromising the primary goal of fouling resistance.

2.5. Hemocompatibility

Recognizing the need for improved blood-contacting materials, we evaluated the hemocompatibility of coated scaffolds designed for vascular grafts and extracorporeal devices under dynamic flow conditions. To evaluate this, scaffolds were exposed to fresh human blood under orbital shear stress to simulate physiological conditions. SEM images shown in **Fig 6** reveal the blood–material interactions, with red blood cells pseudo-colored red and platelets yellow for clarity. The best representative images are shown here, while additional images are provided in Fig. S5. The SEM micrographs reveal that both control and hexapeptide-coated surfaces exhibited low levels of platelet attachment, with the observed platelets primarily in the early sprouting state, indicative of initial activation. In contrast, the tripeptide-coated PU surface showed minimal platelet presence and visible formation of a thick fibrin mesh, while the PLC surface, especially in the control group, demonstrated increased platelet attachment and denser aggregation.

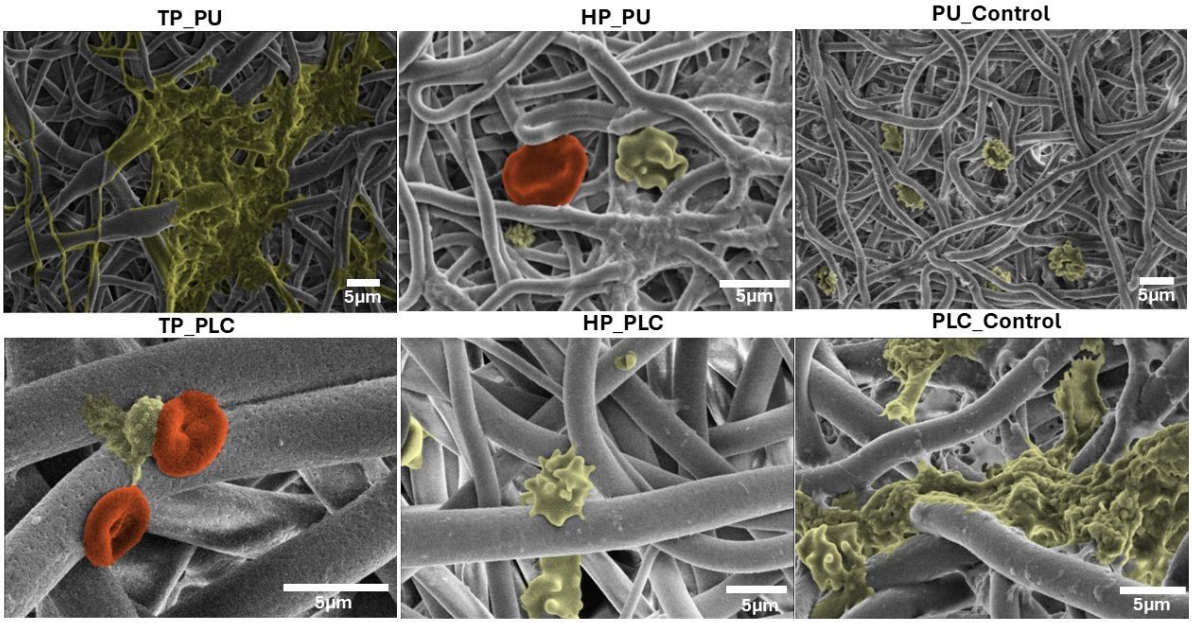

Fig 6. SEM images of platelet and red blood cell (RBC) interactions on unmodified and peptide-functionalized PU and PLC scaffolds. Yellow highlights indicate platelet adhesion and clot formation with visible fibrin mesh networks, while red highlights mark the presence of red blood cells (RBCs). Each scaffold was tested in triplicate (N = 3), with SEM images collected at least 5 random regions per sample

These findings are further supported by hemolysis assays, where all PU and PLC scaffold groups exhibited hemolysis ratios below 5%, indicating good blood

View Article Online
DOI: 10.1039/D6MA00253F

compatibility **(Fig 7).** According to ISO 10993-4 guidelines, values ≤2% are classified as non-hemolytic and safe for implantation, while those between 2–5% are considered slightly hemolytic but still acceptable[56]. Both peptide-functionalized and control scaffolds fell within this acceptable range. Although peptide-coated samples showed slightly reduced hemolysis compared to controls, statistical analysis using Student's t-test revealed no significant differences. Together, these results confirm that peptide immobilization does not compromise the hemocompatibility of scaffolds.

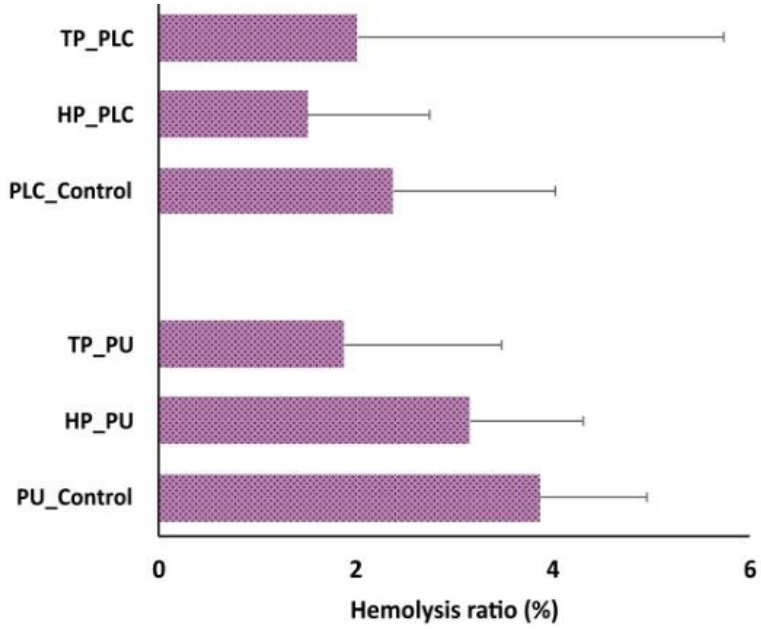

Fig 7. Quantitative hemolysis analysis confirms no blood damage across all samples, indicating good hemocompatibility. No significant differences observed between groups ($p > 0.05$, Student's t-test), Data are mean ± SD ($n = 3$ technical replicates per condition; $N = 3$ independent biological repeats).

SEM imaging revealed multiple stages of blood clot formation, from early platelet activation with filopodia extension to intermediate platelet clustering and fibrin sprouting, culminating in dense fibrin networks and thrombus-like structures. More images provided in Supplementary data (Fig S5). Notably, peptide-coated PLC surfaces exhibited fewer fibrin strands than controls, highlighting the coating's ability to modulate platelet response while minimizing excessive clotting.

To assess the hemostatic compatibility of the base scaffold materials, only unmodified PU and PLC scaffolds subjected to Prothrombin Time (PT) and Partial Thromboplastin Time (PTT) assays. This decision was based on prior hemolysis results, which showed that peptide immobilization did not induce any adverse blood-related effects. Therefore, the coagulation assessment focused solely on the control scaffolds to establish the intrinsic compatibility of the

View Article Online
DOI: 10.1039/D6MA00253F

base polymers. PT assesses the extrinsic and common pathways, while PTT evaluates the intrinsic and common pathways of the coagulation cascade, critical for preventing both excessive bleeding and unwanted clot formation.[57]

The PT values across all scaffold groups ranged from 90% to 97%, staying close to the physiological baseline. Similarly, PTT values remained stable, between 26 and 27 seconds, showing no significant deviations.[58] These results indicate that neither peptide immobilization nor scaffold composition induced abnormal coagulation, confirming blood compatibility and hemostatic safety following biomaterials standards. [59]

3. Conclusion

This study demonstrates key advances in surface engineering of polymeric biomaterials. First, While DOPA-based coatings are well established for metallic systems, their application to polymeric substrates remains less explored due to challenges associated with lower surface energy. Here, we demonstrate effective peptide immobilization on electrospun polymer scaffolds. Second, the combination of antifouling and bio-interactive (RGD-mediated) functionalities within a single platform, along with evaluation under dynamic conditions, provides insight into their potential for biomedical applications. Finally, the use of LC–MS for quantifying surface-bound peptides following extraction offers a sensitive analytical approach for characterizing such systems. Overall, these findings contribute to the development of peptide-functionalized polymeric biomaterials and may contribute to future design strategies for hemocompatible applications.

4. Experimental Section

Materials

Pellethane 2363-80AE (PU) purchased from Lubrizol (Cleveland, OH, USA). 1,1,1,3,3,3-Hexafluoro-2-isopropanol (HFIP, ≥99%) obtained from Fluorochem (Hadfield, UK). PURASORB® PLC 7015 (75:30 mol% L-lactide: ε-caprolactone) Poly(L-lactide-co-ε-caprolactone) (PLC) copolymer, obtained from Corbion, Netherlands.Dichloromethane (DCM, HPLC grade) purchased from Merck (Darmstadt, Germany). Peptides DOPA-Phe(4F)-Phe(4F)-COOMe and DOPA-Phe(4F)-Phe(4F)-RGD were synthesized, purified and characterized based on previous protocols [17,18] Tris buffer (Tris hydrochloride, electrophoresis grade, ≥99.9%) was purchased from Sigma-

View Article Online
DOI: 10.1039/D6MA00253F

Aldrich (St. Louis, MO, USA). Glutaraldehyde (25% aqueous solution) purchased from Thermo Scientific – Alfa Aesar. Absolute ethanol (≥99.5%) purchased from Sigma-Aldrich (St. Louis, MO, USA). Iridium sputter coating targets (99.9% purity) obtained from Ted Pella, Inc. (Redding, CA, USA). F-12 HAM cell culture medium, fetal bovine serum (FBS, heat-inactivated), penicillin-streptomycin-amphotericin solution, trypsin-EDTA solution (sterile, DNase/RNase/protease free), and Dulbecco's phosphate buffered saline (PBS, pH 7.4) were purchased from Biological Industries (Beit Haemek, Israel). Chinese hamster ovary cells (CHO-K1, ATCC CCL-61) and *Staphylococcus epidermidis* (ATCC 12228), *Staphylococcus aureus* (ATCC 29213), and *Escherichia coli* (ATCC 25922) obtained from American Type Culture Collection (ATCC, Manassas, VA, USA). Lysogeny Broth (LB) powder, MHB purchased from Becton Dickinson (Franklin Lakes, NJ, USA). Nutrient agar powder for microbiology purchased from Merck (Darmstadt, Germany). Proteinase K (molecular biology grade, DNase/RNase/protease free), ascorbic acid (≥99%, analytical grade), and calcium chloride dihydrate ($CaCl_2 \cdot 2H_2O$, analytical grade) purchased from Sigma-Aldrich (St. Louis, MO, USA). Fresh whole human blood collected from healthy volunteers under approved ethical guidelines. All statistical analyses performed using Microsoft Excel (Microsoft Office 365, USA) unless otherwise mentioned.

Peptide synthesis

The hexapeptide DOPA-Phe(4F)-Phe(4F)-RGD was synthesized via standard solid-phase peptide synthesis (SPPS) on a 0.25 mmol scale using Rink amide resin, following previously reported protocols with minor modifications. [17] The purified peptide was obtained with a purity of 97%. The DOPA-Phe(4F)-Phe(4F)-COOMe was synthesized via solution-phase peptide synthesis as previously reported. [17,18]Briefly, peptide coupling reactions were carried out using DCC/HOBt-mediated activation in dry dichloromethane, followed by sequential deprotection and purification steps. The final product was characterized by MALDI-TOF mass spectrometry and NMR spectroscopy prior to use and was obtained with 98% purity.

Electrospinning technique for polymer scaffolds preparation

Electrospinning performed using a NANON 01A vertical electrospinning device (MECC Co. Instruments Ltd., Fukuoka, Japan). Polymer solutions were prepared by dissolving 5% w/v PU in HFIP, and 20% w/v PLC, in DCM. Each polymer solution

View Article Online
DOI: 10.1039/D6MA00253F

extruded through a 22-gauge blunt-tip needle at a feed rate of 0.6 mL/h, a needle-to-collector distance of 15 cm, and an applied voltage of 20 kV. Environmental parameters maintained at 27 °C and 35% relative humidity. Electrospinning conducted on a flat stationary collector for 1 hour, yielding nanofibrous scaffolds with a minimum thickness of 100 µm. The resulting scaffolds stored in a desiccator at room temperature until further use.

Peptide Immobilization on Polymer Scaffold

Scaffold surface functionalization conducted by incubating 1 cm² electrospun PU and PLC scaffolds with peptide solutions. DOPA-Phe(4F)-Phe(4F)-COOMe (1 mg/mL) dissolved in ethanol, and DOPA-Phe(4F)-Phe(4F)-RGD (1 mg/mL) dissolved in Tris buffer (pH 7.4, 154 mM ionic strength). Scaffolds incubated with the respective solutions for 48 hours. Following incubation, samples treated in ethanol-based peptide solutions were washed with ethanol to remove unbound peptides and dried under nitrogen. For samples incubated in Tris buffer, scaffolds were first washed with fresh Tris buffer to remove loosely bound peptide, followed by ethanol washing to facilitate drying, and then dried under a nitrogen.

4.1. Characterisation technique

Scanning Electron Microscopy

High-resolution scanning electron microscopy (SEM) imaging performed using an XHR SEM Magellan (Thermo Fisher Scientific, Waltham, MA, USA), equipped with a monochromated Schottky-type field emission gun (FEG) and multiple electron detectors for both SEM and STEM modes. Imaging conducted on 1 cm² electrospun scaffolds sputter-coated with a thin layer of iridium using an accelerating voltage range of 1–30 kV, achieving sub-nanometer resolution. A beam decelerator allowed landing energies as low as 50 eV to enhance surface sensitivity. For each scaffold, at least three different regions scanned to obtain representative average morphological data. Fiber diameter measurements conducted using ImageJ software with a sample size of N = 50 fibers per group.

ATR-FTIR Spectroscopy

Attenuated Total Reflectance Fourier Transform Infrared (ATR-FTIR) spectra obtained using a Nicolet iS20 spectrometer (Thermo Fisher Scientific, Waltham, MA, USA) over the 4000–500 cm^{-1} range, with 32 scans collected at a resolution of 4 cm^{-1}. FTIR

View Article Online
DOI: 10.1039/D6MA00253F

analysis performed on electrospun (1cm^2) PU and PLC scaffolds before and after surface peptide functionalization to assess chemical modifications.

Surface wettability

Static water contact angle measurements were performed on electrospun PU scaffold before and after coating using a Contact Angle Meter (DMe-211, Kyowa Interface Science). Mats (1 × 1 cm) were mounted using adhesive tape, and 5 μL droplets of bi-distilled water were deposited onto the surface. Images were captured immediately, and contact angles were calculated using FAMAS software (v3.3). All measurements were conducted at 22–25 °C.

X-ray photoelectron spectroscopy

X-ray photoelectron spectroscopy (XPS) measurements performed using Kratos AXIS Supra spectrometer (Kratos Analytical Ltd., Manchester, U.K.) with Al Kα monochromatic radiation X-ray source (1486.6 eV). The XPS spectra acquired with a take-off angle of 90° (normal to analyzer); vacuum condition in the chamber was 2×10^{-9} Torr. The high-resolution XPS spectra of C 1s, O 1s, N 1s and F 1s measured with pass energy of 20 and 0.1 eV step size. The binding energies calibrated using C 1s peak energy as 285.0 eV. Data collected and analyzed by using ESCAPE processing programs (Kratos Analytical Ltd, Manchester, U.K) and Casa XPS (Casa Software Ltd, Manchester, U.K). Due to the inherent fragility of electrospun scaffolds, sample mounting for XPS performed with caution to prevent structural damage. To maintain scaffold integrity, separate specimens used for pre- and post-treatment analyses, with minor variability attributed to inter-sample differences.

Quantification of peptide on the Surface using Liquid Chromatography-Mass Spectrometer

Peptide functionalized scaffolds incubated for 4 hrs. in a digestion solution containing Proteinase K (1 mg/mL), supplemented with 5 mM ascorbic acid and 5 mM $CaCl_2$ to preserve enzymatic activity. This enzymatic treatment facilitates the release of surface-bound peptides for quantification by digesting the peptide bonds. The reaction was stopped by freezing it in -80˚C. Peptide immobilization estimated by measuring the released 4-fluorophenylalanine (4F-Phe), serving as a marker for peptide identification. Media samples (20 μL) were mixed with 180 μL of extraction buffer

View Article Online
DOI: 10.1039/D6MA00253F

(MeOH:MeCN:H_2O, 5:3:2), vortexed for 1 min, and centrifuged at 13,000 RPM for 20 min at 4 °C. Supernatants were transferred to HPLC vials for LC-MS analysis. Calibration curves were prepared using 4F-Phe standards (0.0054–5.464 μM) diluted in extraction buffer.

LCMS metabolomics analysis was performed as described previously.[60] Dionex Ultimate 3000 UPLC system coupled to an Orbitrap Q-Exactive Plus MS (Thermo Fisher Scientific, Waltham, MA, USA) with a resolution of 70,000 at 200 mass/charge ratio (m/z)electrospray ionization in the HESI source, and polarity switching mode to enable both positive and negative ions across a mass range of 70 to 1000 m/z, was used. The UPLC setup included a ZIC-pHILIC column (SeQuant; 150 mm × 2.1 mm, 5 μm; Merck) with a Sure-Guard filter (SS frit 0.5 μm). Five μL of the tissue extracts were injected and the compounds were separated with a mobile phase gradient of 15 min, starting at 20% aqueous (20 mM ammonium carbonate adjusted to pH 9.2 with 0.1% of 25% ammonium hydroxide) and 80% organic (acetonitrile) and terminated with 20% acetonitrile. The flow rate and column temperature were maintained at 0.2 mL/min and 45 °C, respectively, for a total run time of 26 min. All metabolites were detected using mass accuracy below 5 ppm. Data acquired with Thermo Xcalibur. Metabolites quantified in Trace Finder 5.2 using calibration curves appropriate to concentration range. For full-range samples (0.0054–5.464 μM), the calibration equation (1). The Data normalized to sample optical density (OD), with averages calculated from three replicates (n = 3).

$$y = 9 \times 10^6 x + 1 \times 10^6 \, (R^2 = 0.9933) \quad - (1)$$

In Vitro Cell Adhesion and Viability

Experiments performed using Chinese hamster ovary cells (CHO-K1, ATCC CCL-61). For cell adhesion and proliferation studies, CHO cells were cultured in F-12 HAM medium supplemented with 10% (v/v) fetal bovine serum (FBS), 100 U/mL Penicillin, 0.1 mg/mL Streptomycin, and 0.25 μg/mL Amphotericin. Cells were maintained at 37 °C in a humidified incubator with 5% CO_2. Upon reaching approximately 80% confluence, cells detached using Trypsin-EDTA (B) and proceeded for subculture. The culture medium refreshed between passages. All experiments conducted using cells at passages 3 to 6.

Trypan Blue Assay and SEM Visualization of Cells

View Article Online
DOI: 10.1039/D6MA00253F

CHO cells (25,000 cells/mL) were seeded onto 2 cm² UV-sterilized electrospun scaffolds of PU and PLC, including their respective peptide-functionalized variants, and incubated for 72 hours. Post-incubation, cells were Trypsinated, stained with trypan blue, and counted using a hemocytometer. The cell count was determined by counting live and dead cells separately, and the number of viable and non-viable cells calculated according to the equation (2). All experiments performed in triplicate across three independent biological replicates (n = 3, N = 3), and data presented as mean ± standard deviation. Statistical significance between groups was determined using a two-tailed Student's *t*-test, with $p < 0.05$ considered statistically significant.

$$\text{Cell Count} = \frac{\text{Average Cell Count per Square} \times \text{Dilution Factor} \times \text{Total Volume}}{\text{Volume of One Square}} \quad -(2)$$

Cell morphology analysis on the scaffolds performed after fixation with 3% glutaraldehyde and stepwise dehydration using ethanol solutions (30%, 50%, 70%, 90%, and 100%). Samples air-dried in a biosafety cabinet and sputter-coated with iridium prior to SEM imaging. At least five random regions of interest (ROIs) selected per scaffold for analysis.

Bacterial Adhesion Quantification

Bacterial strains cultured overnight at 37 °C under shaking conditions (120 rpm) in appropriate nutrient media: E. coli in LB broth, and S. epidermidis and S. aureus in MHB. Overnight cultures diluted to a final concentration of 10^5 CFU/mL in fresh broth medium before use and confirmed by optical density measurement at 600 nm using a UV-1650PC spectrophotometer (Shimadzu, Kyoto, Japan). Electrospun scaffolds (1 cm²) made of PU, PLC, and their corresponding peptide-functionalized surfaces sterilized under UV for 30min and placed individually into 24-well plates. A 1 mL aliquot of each bacterial suspension added to the scaffolds and incubated at 37 °C for 24 hr. to allow bacterial adhesion and early biofilm formation. Following incubation, scaffolds gently rinsed once with sterile phosphate-buffered saline (PBS) to remove non-adherent bacteria. Adherent bacteria were detached by sonication in a water bath sonicator for 15 min, followed by vortexing for 15 s. The recovered bacterial suspensions were serially diluted (10-fold) in sterile PBS, and 5 µL from each dilution was dropped onto Nutrient Agar plates (prepared by following manual instruction 11.5 g in 500mL of distilled water The medium was sterilized by autoclaving at 121 °C for 15 min, cooled

View Article Online
DOI: 10.1039/D6MA00253F

to approximately 50 °C, poured into sterile Petri dishes under aseptic conditions and allowed to solidify). Plates incubated at 37 °C overnight, and bacterial colonies counted the following day. Results reported as colony-forming units per scaffold. The total colony forming unit (CFU) calculated using the following equation:

$$\text{Total CFU} = \frac{(\text{Number of colonies} \times \text{Total recovered Volume (mL)})}{(\text{Dilution factor} \times \text{Volume plated (mL)})} \quad -(3)$$

This formula accounts for the 1 mL of recovered bacterial suspension following sonication and vortexing, and the 5 µL plated on nutrient agar. All experiments were performed in triplicate across three independent biological replicates (n = 3, N = 3). Statistical significance between groups was determined using one-way ANOVA with Tukey–Kramer post hoc test (*$p < 0.05$, **$p < 0.01$, ***$p < 0.001$).

For morphological analysis, scaffolds fixed in 3% glutaraldehyde at 4 °C for 2 h and dehydrated through a graded ethanol series (30%, 50%, 70%, 90%, 100%, 10 min each step). Samples dried, sputter-coated with iridium, and imaged using high-resolution scanning electron microscopy to visualize bacterial attachment.

Hemocompatibility Evaluation

Blood samples were obtained from healthy donors (n = 3) in accordance with the Hadassah–Hebrew University Medical Center Ethics Board guidelines (Protocol HMO-0637-08: "Evaluation of platelet function using the Impact-R cone and platelet analyzer"), following signed informed consent. Whole blood was collected in sodium citrate tubes and rested for 1 h before use. Platelet adhesion was assessed using the DiaMed Impact-R cone and plate analyzer (DiaMed GmbH, Switzerland). A 0.13 mL aliquot of fresh whole blood was exposed to the scaffold surfaces under a shear rate of 1800 s^{-1} for 2 min. After incubation, samples were washed with PBS, fixed following the same protocol used for cell and bacterial adhesion studies, sputter-coated with iridium, and imaged by SEM to evaluate platelet adhesion and morphology. Experiments were performed with fresh blood from three donors in three independent runs. Each scaffold was tested in triplicate (N = 3), with SEM images collected atleast 5 random regions per sample.

Coagulation and Hemolysis Tests

View Article Online
DOI: 10.1039/D6MA00253F

Electrospun PU and PLC scaffolds (0.5 cm²) were incubated with fresh human blood at 37 °C for 30 minutes. Following incubation, the samples were centrifuged to separate the plasma. The collected plasma analyzed for prothrombin time (PT) and partial thromboplastin time (PTT) using a Sysmex CS-5100 coagulation analyzer (Sysmex Corporation, Nagasaki, Japan). Hemolysis assessed by measuring the absorbance of the separated plasma (supernatant) transferred to a 96-well plate and read at 540 nm using the integrated UV-Vis spectrophotometer of the SQII® ELISA PROCESSOR (AESKU Diagnostics, Germany), to evaluate red blood cell lysis. All experiments performed in triplicate across three independent biological replicates (n = 3, N = 3), and data presented as mean ± standard deviation. Statistical significance between groups was determined using a two-tailed Student's *t*-test, with $p < 0.05$ considered statistically significant. All statistical analyses performed using Microsoft Excel (Microsoft Office 365, USA).

Acknowledgements

Funding: This project funded by the European Union's research and innovation program under the Marie Sklodowska-Curie grant agreement No 101072645.

Conflicts of interest

There are no conflicts to declare.

Data Availability Statement

The raw data of this publication are available on the Dataverse website at the link: https://dataverse.unimi.it/dataverse/HUJI-UNIPV-AN-1.

Ethics approval statement

Human blood collection and use were approved by the Hadassah–Hebrew University Medical Center Ethics Board (Protocol HMO-0637-08). All donors provided informed consent prior to participation.

References

1. *Global burden of bacterial antimicrobial resistance in 2019: a systematic analysis.* Lancet, 2022. **399**(10325): p. 629-655.
2. Campoccia, D., L. Montanaro, and C.R. Arciola, *A review of the biomaterials technologies for infection-resistant surfaces.* Biomaterials, 2013. **34**(34): p. 8533-54.
3. de la Fuente-Nunez, C., A. Cesaro, and R.E.W. Hancock, *Antibiotic failure: Beyond antimicrobial resistance.* Drug Resist Updat, 2023. **71**: p. 101012.

4. Kaganovich, M., et al., *Fabrication of antimicrobial polymeric films by compression molding of peptide assemblies and polyethylene.* Chemical Communications, 2022. **58**(67): p. 9357-9360.
5. Le, H., et al., *Antibody-Conjugated Nanocarriers for Targeted Antibiotic Delivery: Application in the Treatment of Bacterial Biofilms.* Biomacromolecules, 2021. **22**(4): p. 1639-1653.
6. Hetrick, E.M. and M.H. Schoenfisch, *Reducing implant-related infections: active release strategies.* Chemical Society Reviews, 2006. **35**(9): p. 780-789.
7. Cernohorsky, P., et al., *The relevance of aortic endograft prosthetic infection.* J Vasc Surg, 2011. **54**(2): p. 327-33.
8. Oda, T., et al., *Prosthetic vascular graft infection through a median sternotomy: a multicentre review †.* Interact Cardiovasc Thorac Surg, 2015. **20**(6): p. 701-6; discussion 706.
9. Sixt, T., et al., *Long-term Prognosis Following Vascular Graft Infection: A 10-Year Cohort Study.* Open Forum Infectious Diseases, 2022. **9**(4).
10. Stockschläder, L., et al., *Characteristics and Outcome of Vascular Graft Infections: A Risk Factor and Survival Analysis.* Open Forum Infectious Diseases, 2024. **11**(6).
11. Anderson, T.H., et al., *The Contribution of DOPA to Substrate-Peptide Adhesion and Internal Cohesion of Mussel-Inspired Synthetic Peptide Films.* (1616-301X (Print)).
12. Ou, X., et al., *Structure and sequence features of mussel adhesive protein lead to its salt-tolerant adhesion ability.* Science Advances. **6**(39): p. eabb7620.
13. Asha, A.B., et al., *Rapid Mussel-Inspired Surface Zwitteration for Enhanced Antifouling and Antibacterial Properties.* Langmuir, 2019. **35**(5): p. 1621-1630.
14. Zanuy, D., et al., *Structural preferences of an anti-fouling peptide: From single chain to small molecular assemblies.* Biophysical Chemistry, 2021. **272**: p. 106555.
15. Lee, H., et al., *Mussel-inspired surface chemistry for multifunctional coatings.* Science, 2007. **318**(5849): p. 426-30.
16. Maity, S., et al., *Self-assembly of a tripeptide into a functional coating that resists fouling.* Chemical Communications, 2014. **50**(76): p. 11154-11157.
17. Yu, J., et al., *Mussel protein adhesion depends on interprotein thiol-mediated redox modulation.* Nat Chem Biol, 2011. **7**(9): p. 588-90.
18. Yuran, S., A. Dolid, and M. Reches, *Resisting Bacteria and Attracting Cells: Spontaneous Formation of a Bifunctional Peptide-Based Coating by On-Surface Assembly Approach.* ACS Biomaterials Science & Engineering, 2018. **4**(12): p. 4051-4061.
19. Das, P. and M. Reches, *Revealing the role of catechol moieties in the interactions between peptides and inorganic surfaces.* Nanoscale, 2016. **8**(33): p. 15309-15316.
20. Maity, S., et al., *Self-Assembly af a Tripeptide into a Functional Coating that Resists Fouling.* Chem. Commun., 2014. **50**(76): p. 11154.
21. Yuran, S. and M. Reches, *Formation of ordered biomolecular structures by the self-assembly of short peptides.* J Vis Exp, 2013(81): p. e50946.
22. Chernonosova, V., et al., *Assessment of Electrospun Pellethane-Based Scaffolds for Vascular Tissue Engineering.* Materials, 2021. **14**(13): p. 3678.
23. Zhu, Y., et al., *Progress in the development of self-healing polyurethane materials.* Resources Chemicals and Materials, 2025. **4**(3): p. 100114.
24. Mun, C.H., et al., *Three-dimensional electrospun poly(lactide-co-ε-caprolactone) for small-diameter vascular grafts.* Tissue Eng Part A, 2012. **18**(15-16): p. 1608-16.
25. Fu, Z., et al., *Development and challenges of cells- and materials-based tooth regeneration.* Engineered Regeneration, 2022. **3**(2): p. 163-181.
26. Agarwal, S., J.H. Wendorff, and A. Greiner, *Use of electrospinning technique for biomedical applications.* Polymer, 2008. **49**(26): p. 5603-5621.

View Article Online
DOI: 10.1039/D6MA00253F

27. Li, D. and Y. Xia, *Electrospinning of Nanofibers: Reinventing the Wheel?* Advanced Materials, 2004. **16**(14): p. 1151-1170.
28. Pham, Q.P., U. Sharma, and A.G. Mikos, *Electrospinning of polymeric nanofibers for tissue engineering applications: a review.* Tissue Eng, 2006. **12**(5): p. 1197-211.
29. organisation, W.H., *Antimicrobial Resistance Division (AMR), Surveillance, Prevention and Control (SPC)*.
30. Wiffen, P., *Keeping the focus on antimicrobials.* Eur J Hosp Pharm, 2022. **29**(e1): p. e1.
31. Barth, A., *Infrared spectroscopy of proteins.* Biochim Biophys Acta, 2007. **1767**(9): p. 1073-101.
32. Kaganovich, M., et al., *Spontaneous Formation of a Sustainable Antifreeze Coating by Peptide Self-Assembly.* ACS Applied Materials & Interfaces, 2025. **17**(10): p. 16256-16267.
33. van den Broek, I., et al., *Quantitative bioanalysis of peptides by liquid chromatography coupled to (tandem) mass spectrometry.* J Chromatogr B Analyt Technol Biomed Life Sci, 2008. **872**(1-2): p. 1-22.
34. Erdőssy, J., et al., *Enzymatic digestion as a tool for removing proteinaceous templates from molecularly imprinted polymers.* Analytical Methods, 2017. **9**(31): p. 4496-4503.
35. Gong, X., et al., *Desalting by crystallization: detection of attomole biomolecules in picoliter buffers by mass spectrometry.* Anal Chem, 2015. **87**(19): p. 9745-51.
36. Hilz, H., U. Wiegers, and P. Adamietz, *Stimulation of proteinase K action by denaturing agents: application to the isolation of nucleic acids and the degradation of 'masked' proteins.* Eur J Biochem, 1975. **56**(1): p. 103-8.
37. BAJORATH, J., W. HINRICHS, and W. SAENGER, *The enzymatic activity of proteinase K is controlled by calcium.* European Journal of Biochemistry, 1988. **176**(2): p. 441-447.
38. Ito, S., et al., *Oxidation of tyrosine residues in proteins by tyrosinase. Formation of protein-bonded 3,4-dihydroxyphenylalanine and 5-S-cysteinyl-3,4-dihydroxyphenylalanine.* Biochem J, 1984. **222**(2): p. 407-11.
39. Ebeling, W., et al., *Proteinase K from Tritirachium album Limber.* Eur J Biochem, 1974. **47**(1): p. 91-7.
40. Sierevogel, M.J., et al., *Matrix metalloproteinases: a therapeutic target in cardiovascular disease.* Curr Pharm Des, 2003. **9**(13): p. 1033-40.
41. Turk, V., et al., *Cysteine cathepsins: from structure, function and regulation to new frontiers.* Biochim Biophys Acta, 2012. **1824**(1): p. 68-88.
42. Visse, R. and H. Nagase, *Matrix metalloproteinases and tissue inhibitors of metalloproteinases: structure, function, and biochemistry.* Circ Res, 2003. **92**(8): p. 827-39.
43. Dillon, J.G., *Electrochemical degradation of Pellethane 2363-80A and 2363-55D.* Polymer Degradation and Stability, 1992. **37**(3): p. 183-188.
44. Das, P. and M. Reches, *Revealing the Role of Catechol Moieties in the Interactions Between Peptides and Inorganic Surfaces.* Nanoscale, 2016. **8**(33): p. 15309.
45. Bayramoglu, G., et al., *Hydrophilic spacer-arm containing magnetic nanoparticles for immobilization of proteinase K: Employment for speciation of proteins for mass spectrometry-based analysis.* Talanta, 2020. **206**: p. 120218.
46. Vanaman Wilson, M.J., J. Bolton, and S.G. Fabi, *A randomized, single-blinded trial of a tripeptide/hexapeptide healing regimen following laser resurfacing of the face.* J Cosmet Dermatol, 2017. **16**(2): p. 217-222.
47. Rigler, P., et al., *Reversible immobilization of peptides: surface modification and in situ detection by attenuated total reflection FTIR spectroscopy.* Chemphyschem, 2003. **4**(3): p. 268-75.

48. Mak, S.Y., et al., *A simple and highly sensitive LC–MS workflow for characterization and quantification of ADC cleavable payloads.* Scientific Reports, 2024. **14**(1): p. 11018.
49. Zhang, W., et al., *Molecular interactions between DOPA and surfaces with different functional groups: a chemical force microscopy study.* RSC Advances, 2017. **7**(52): p. 32518-32527.
50. Guvendiren, M., et al., *Adhesion of DOPA-Functionalized Model Membranes to Hard and Soft Surfaces.* J Adhes, 2009. **85**(9): p. 631-645.
51. Anderson, J.M., D.T. Rodriguez A Fau - Chang, and D.T. Chang, *Foreign body reaction to biomaterials.* (1044-5323 (Print)).
52. 194, I.T., *ISO 10993-5:2009 Biological evaluation of medical devices Part 5: Tests for in vitro cytotoxicity*. 2009-06. p. 34.
53. Lim, M.M., T. Sun, and N. Sultana, *In Vitro Biological Evaluation of Electrospun Polycaprolactone/Gelatine Nanofibrous Scaffold for Tissue Engineering.* Journal of Nanomaterials, 2015. **2015**(1): p. 303426.
54. Hersel, U., C. Dahmen, and H. Kessler, *RGD modified polymers: biomaterials for stimulated cell adhesion and beyond.* Biomaterials, 2003. **24**(24): p. 4385-415.
55. Massia, S.P. and J.A. Hubbell, *An RGD spacing of 440 nm is sufficient for integrin alpha V beta 3-mediated fibroblast spreading and 140 nm for focal contact and stress fiber formation.* Journal of Cell Biology, 1991. **114**(5): p. 1089-1100.
56. 194, I.T., *ISO 10993-4:2017 Biological evaluation of medical devices Part 4: Selection of tests for interactions with blood*. International Standard Organisation. p. 69.
57. Palta, S., R. Saroa, and A. Palta, *Overview of the coagulation system.* Indian J Anaesth, 2014. **58**(5): p. 515-23.
58. Rountree, K.M., Z. Yaker, and P.P. Lopez, *Partial Thromboplastin Time*, in *StatPearls*. 2026, StatPearls Publishing Copyright © 2026, StatPearls Publishing LLC.: Treasure Island (FL) ineligible companies. Disclosure: Zachary Yaker declares no relevant financial relationships with ineligible companies. Disclosure: Peter Lopez declares no relevant financial relationships with ineligible companies.
59. Ayyar, M., et al., *Preparation, characterization and blood compatibility assessment of a novel electrospun nanocomposite comprising polyurethane and ayurvedic-indhulekha oil for tissue engineering applications.* Biomed Tech (Berl), 2018. **63**(3): p. 245-253.
60. Mackay, G.M., et al., *Analysis of Cell Metabolism Using LC-MS and Isotope Tracers.* Methods Enzymol, 2015. **561**: p. 171-96.

View Article Online
DOI: 10.1039/D6MA00253F

Data availability

The raw data for this publication are available on the Dataverse website at the following link: https://dataverse.unimi.it/dataverse/HUJI-UNIPV-AN-1.